Hydrol. Earth Syst. Sci. Discuss., 11, 723–756, 2014
www.hydrol-earth-syst-sci-discuss.net/11/723/2014/
doi:10.5194/hessd-11-723-2014

Hydrology and Earth System Sciences
Open Access
Discussions

Evaluating the SSEBop approach for evapotranspiration mapping with landsat data using lysimetric observations in the semi-arid Texas High Plains

G. B. Senay[1], P. H. Gowda[2], S. Bohms[3], T. A. Howell[2], M. Friedrichs[3], T. H. Marek[4], and J. P. Verdin[1]

[1]US Geological Survey (USGS), Earth Resources Observation and Science (EROS) Center, Sioux Falls, South Dakota, USA
[2]US Department of Agriculture- Agriculture Research Service (USDA-ARS) Conservation and Production Research Laboratory, Bushland, Texas, USA
[3]SGT, Inc. contractor to USGS EROS, Sioux Falls, South Dakota, USA
[4]Texas A&M AgriLife Research, Amarillo, Texas, USA

Received: 1 November 2013 – Accepted: 11 December 2013 – Published: 15 January 2014

Correspondence to: G. B. Senay (senay@usgs.gov)

Published by Copernicus Publications on behalf of the European Geosciences Union.

Abstract

The operational Simplified Surface Energy Balance (SSEBop) approach was applied on 14 Landsat 5 thermal infrared images for mapping daily actual evapotranspiration (ETa) fluxes during the spring and summer seasons (March–October) in 2006 and 2007. Data from four large lysimeters, managed by the USDA-ARS Conservation and Production Research Laboratory were used for evaluating the SSEBop estimated ETa. Lysimeter fields are arranged in a 2 × 2 block pattern with two fields each managed under irrigated and dryland cropping systems. The modeled and observed daily ETa values were grouped as "irrigated" and "dryland" at four different aggregation periods (1-day, 2-day, 3 day and "seasonal") for evaluation. There was a strong linear relationship between observed and modeled ETa with R^2 values ranging from 0.87 to 0.97. The root mean square error (RMSE), as percent of their respective mean values, were reduced progressively with 28, 24, 16 and 12 % at 1-day, 2-day, 3-day, and seasonal aggregation periods, respectively. With a further correction of the underestimation bias (−11 %), the seasonal RMSE reduced from 12 to 6 %. The random error contribution to the total error was reduced from 86 to 20 % while the bias' contribution increased from 14 to 80 % when aggregated from daily to seasonal scale, respectively. This study shows the reliable performance of the SSEBop approach on the Landsat data stream with a transferable approach for use with the recently launched LDCM (Landsat Data Continuity Mission) Thermal InfraRed Sensor (TIRS) data. Thus, SSEBop can produce quick, reliable and useful ET estimations at various time scales with higher seasonal accuracy for use in regional water management decisions.

1 Introduction

Evapotranspiration (ET) is an important process in the hydrologic cycle. Among the major water budget components, ET is in a gaseous state as opposed to precipitation and stream flow; thus, making it the most difficult component to measure directly. ET

HESSD
11, 723–756, 2014

comprises evaporation from the soil and vegetation surfaces and transpiration from the plants. Consequently, it plays a major role in the exchange of mass and energy between the soil–water–vegetation system and the atmosphere. Knowledge of the rate and amount of ET for a given location is an essential component in the design, development, and monitoring of hydrologic, agricultural, and environmental systems. For example, ET is a key variable in irrigation scheduling (Porter et al., 2012), water allocation (Bastiannssen et al., 2012), crop modeling (Thenkabail, 2003), understanding of water dynamics in wetlands (Oberg and Melesse, 2006), and quantifying energy-moisture exchange between the land surface and the atmosphere (Anderson, 1997). The increasing availability of remotely sensed data for monitoring vegetation conditions (Tucker, 1979), estimation of rainfall (Xie and Arkin, 1997), and land surface temperature (Wan and Li, 1997; Chaves et al., 2009) has led to the development of various water balance and energy balance techniques to quantify and map ET at various temporal and spatial scales (Gowda et al., 2008). The choice of the specific approach appears to depend on the availability of data and the intended use of the ET products (Senay et al., 2011).

Surface energy balance methods have been developed and used by several researchers (Jackson et al., 1981; Moran et al., 1996; Anderson et al., 1997; Bastiaanssen et al., 1998; Kustas and Norman, 2000; Roerink et al., 2000; Su, 2002; Allen et al., 2007; Senay et al., 2007) to estimate agricultural crop water use and landscape ET. A comprehensive summary of the various surface energy balance models is presented by Gowda et al. (2008) and Kalma et al. (2008). Senay et al. (2011) specifically summarized the application of the different methods for basin-scale ET estimation. Allen et al. (2011) also provided a succinct review of remote sensing energy balance models with respect to other ET measurement methods, including their expected accuracy.

1.1 Justification

The simplified surface energy balance approach (SSEB; Senay et al., 2007) has evolved from a focus on large irrigation basins (uniform hydro climatic zones) to

HESSD
11, 723–756, 2014

a continent scale with diverse ecosystems (Senay et al., 2013). The continental application was made possible with an innovative parameterization using pre-defined hot and cold boundary conditions, which prompted the renaming of the model with the suffix "op" (SSEBop) to indicate its potential use for routine operational applications (Senay et al., 2013). This simplicity is particularly important for the US Department of the Interior (DOI)/US Geological Survey's (USGS) WaterSMART (Water for Sustaining Managing America's Resources for Tomorrow) Program to quantify and map year-to-year variability in consumptive water use in irrigated basins in a timely manner, i.e., previous year consumptive water use estimates need to be determined before the new irrigation season starts.

There exit several pioneering and successful ET models (e.g., Trapezoid Method: Moran et al., 1996; SEBAL: Bastiaanssen et al., 1998; S-SEBI: Roerink et al.; SEBS: Su, 2000; Two-Source: Kustas and Norman, 2000; METRIC: Allen et al., 2007; ALEXI: Anderson et al., 2007) that estimate ET mainly as a residual of the surface energy balance terms. The choice of SSEBop development was driven by the need to produce ET maps at a large scale on a regular basis with minimal computational requirements. The SSEBop has been applied on the MODIS (MODerate resolution Imaging Spectroradiometer) data stream to generate operational monthly and annual ET anomaly maps for the conterminous US (CONUS) from 2000 to 2013 for drought monitoring purposes (http://earlywarning.usgs.gov/usewem/eta_energy.php). As a part of that study, SSEBop was evaluated using monthly ET data from 45 AmeriFlux eddy covariance datasets collected in 2005 (Senay et al., 2013). The performance of the model varied from region to region, with R^2 values ranging from 0.56 to 0.90, with a CONUS-wide average R^2 value of 0.64. More recently, Velpuri et al. (2013) conducted a comprehensive evaluation of the SSEBop approach, comparing it with multi-year eddy covariance stations, gridded flux tower data, water-balance-based ET and MOD16 ET (Mu et al., 2011) and concluded the usefulness of a MODIS-scale application of the SSEBop approach for agro-hydrologic applications. Previously, Gowda et al. (2009) evaluated the performance of the earlier version of the SSEBop, (i.e., SSEB) using lysimetric data in

HESSD
11, 723–756, 2014

the semi-arid Texas High Plains. Predicted daily actual ET fluxes accounted for 84 % of the variation in the observed ET with an RMSE of 1.2 mm and a mean bias error of −0.6 mm. However, SSEBop has never been evaluated for estimating ET with Landsat datasets.

The main objective of this study is to evaluate the performance of the newly parameterized SSEBop on Landsat data using the same lysimetric datasets that were used by Gowda et al. (2009). The model performance and uncertainty were quantified at four aggregation periods, ranging from a single day to "seasonal" time scales.

1.2 Study site

This study was conducted within the area covered by Landsat 5's path/row of 31/36 in the Southern Great Plains (parts of the Texas High Plains and northeastern New Mexico), south-central United States (Fig. 1). The climate is semiarid with highly variable rainfall. The annual average rainfall is 475 mm, with 348 mm occurring during the summer growing season. The dominant soil in the study area is classified as a Pullman clay loam (fine, mixed, super active, thermic torrertic Paleustolls) with low permeability. The major crops are corn, grain sorghum, winter wheat, and cotton. The typical summer cropping season (in the study area) starts in May and ends in October.

The SSEBop approach was evaluated using soil water mass change-based daily ET values from four large monolithic precision weighing lysimeters located at the US Department of Agriculture-Agricultural Research Service (USDA-ARS) Conservation and Production Research Laboratory (CPRL) in Bushland, Texas (see Fig. 1, Howell et al., 1995). The CPRL Lysimeter Plots are located in the northeastern corner of the Landsat scene with a plot area of 450 m × 439 m. The geographic coordinates are 35°11′ N, 102°06′ W, and the elevation is 1170 m a.m.s.l.

Dryland cropping systems are managed on the two lysimeter fields to the west and an irrigated cropping system is managed on the two lysimeter fields to the east. Irrigation is conducted with a 10-span lateral move sprinkler system. Daily ET was calculated as the difference between lysimeter mass recorded at 23:30 (Central Standard Time,

HESSD
11, 723–756, 2014

CST) of one day and 23:30 CST of the next day to determine mass losses (from evaporation and transpiration) to which lysimeter mass gains (from irrigation or precipitation) were added. Details of the lysimeter features and operational-interfaces are reported in Gowda et al. (2009).

2 Materials and methods

2.1 SSEBop method

SSEBop does not solve the full energy balance terms; however, it defines the boundary conditions based on clear-sky net radiation balance principles. The SSEBop approach (Senay et al., 2013) pre-defines unique sets of "hot/dry" and "cold/wet" reference values for each pixel unlike the original SSEB formulation which uses a set of reference hot and cold pixel-pairs applicable for a limited, uniform hydro-climatic region. To estimate ET routinely, the only data needed for the SSEBop method are surface temperature (Ts, K), air temperature (Ta, K) and grass reference ET (ETo, mm). The most important simplification is based on the knowledge that the surface energy balance process is mainly driven by the available net radiation (R_n). Since thermal remote sensing is conducted under clear-sky conditions, the SSEBop method assumes a location- and date-specific constant temperature difference (dT, K) between the hot/dry and cold/wet boundary reference points. Furthermore, the cold boundary condition is derived as a fraction of the Ta.

With this simplification, actual ET (ETa) can be estimated using Eq. (1) as a fraction of the ETo. The ET fraction (ET_f) is calculated using Eq. (2).

$$ETa = ET_f \times kETo \quad (1)$$

where ETo is the grass reference ET for the location; k is a coefficient that scales the ETo into the level of a maximum ET experienced by an aerodynamically rougher crop such as alfalfa. A recommended value for k equal to 1.25 was used in this study (Allen

HESSD
11, 723–756, 2014

et al., 2011a).

$$ET_f = \frac{Th - Ts}{Th - Tc} = \frac{Th - Ts}{dT} \quad (2)$$

where Ts is the satellite-observed land surface temperature of the pixel whose ET_f is being evaluated on a given image date. Th is the estimated Ts at the idealized reference "hot/dry" condition of the pixel for the same time period, Tc is the estimated Ts at the idealized "cold/wet" reference point. The difference between Th and Tc is simply the dT. Negative ET_f is set to zero.

In this case, dT is pre-defined for the study location as explained in Senay et al. (2013) using the following formulation. It is calculated under clear-sky assumption and does not change from year to year, but is unique for each day and location.

$$dT = \frac{R_n r_{ah}}{\rho_a C_p} \quad (3)$$

where R_n is clear-sky net radiation; r_{ah} is the aerodynamic resistance to heat flow from a hypothetical bare and dry surface, estimated at $110\,s\,m^{-1}$ (Senay et al., 2013); ρ_a is the density of air ($kg\,m^{-3}$), estimated as a function of air pressure and temperature (Allen et al., 1998); C_p is the specific heat of air at constant pressure ($1.013\,kJ\,kg^{-1}\,°C^{-1}$).

With an algebraic rearrangement of equations 1 to 3, ETa can be formulated as the product of commonly used surface energy balance parameters as shown in Eq. (4).

$$ETa = \frac{\rho_a C_p}{R_n r_{ah}}(Th - Ts) \cdot k \cdot ETo \quad (4)$$

Table 1 shows sample dT values corresponding to 21 image acquisition dates in 2006 and 2007 spring/summer cropping season. The cold boundary condition, Tc, is calculated from Ta as follows: because the satellite thermal data (Ts) is acquired during the

HESSD
11, 723–756, 2014

morning hours at a nominal overpass time of 10:30 a.m., the daily maximum air temperature is more closely related to it than the daily minimum temperature. The maximum air temperature is more readily available from weather datasets than the hourly temperature for large scale applications. After examining the relationship between Ts and daymet (Thornton, 2012) daily maximum air temperature in well-vegetated pixels, where NDVI (Normalized Difference Vegetation Index) is greater than 0.8, a median correction coefficient of 0.983 was established from all Landsat image acquisition dates. Because the lysimeter fields did not have an NDVI > 0.8 during the study period, the average of available pixels (NDVI > 0.8) in the entire Landsat scene was used to arrive at the correction coefficient of 0.983, with both Ts and maximum Ta being expressed in Kelvin (K). Note that this correction factor was found to be 0.993 when the MODIS-based Ts was used for the entire US (Senay et al., 2013). This correction highlights the need for recalculating the coefficient depending on the sensor used to estimate Ts and the source of Ta measurements. Senay et al. (2013) report more details on the procedure used for establishing the correction coefficient.

2.2 Data

The most important datasets required to apply the SSEBop approach are: Ts, Ta, and ETo. A brief description of the input datasets is presented below.

Grass Reference ET (ETo): hourly weather data from the Bushland weather station were used to generate daily ETo for 2006 and 2007 using the REF-ET Calculation Software (Allen et al., 2011a) with the standardized Penman–Monteith output option. Table 1 summarizes the ETo and daily maximum air temperature datasets used during the study period.

Air Temperature (Ta): the daily maximum air temperature data from Bushland station were used to simulate the cold boundary condition (Tc) using a correction coefficient. We used the daymet gridded, 1 km, (http://daymet.ornl.gov/overview) daily maximum

HESSD
11, 723–756, 2014

air temperature data to develop the static correction coefficient ($c = 0.983$) as it was the only available gridded daily air temperature data that would correspond with the spatially explicit Ts. However, we found a strong linear relationship between daymet and Bushland air temperature data with an R^2 of 0.97 at the study site, suggesting the potential use of daymet Ta would produce comparable results as the station Ta.

Land Surface Temperature (Ts): Land Surface Temperature (Ts) maps were derived from Landsat 5 thermal data. For this purpose, the SSEBop approach incorporated a simple set of hybrid algorithms composed of commonly used calibration steps and atmospheric correction techniques. These include calculations for: (1) spectral radiance conversion to the at-sensor brightness temperature; (2) atmospheric absorption and re-emission value; and (3) surface emissivity.

Ts maps were computed using a modified equation (from Allen et al., 2007) with both atmospheric and surface emissivity calculations using:

$$T_s = \frac{K_2}{[\ln(\varepsilon_{NB} K_1 / R_c) + 1]} \quad (5)$$

where, K_1 and K_2 are prelaunch calibration constants; ε_{NB} is the narrow band emissivity derived from a modification of the NDVI Thresholds Method – NDVI^{THM} (Jiménez-Muñoz and Sobrino, 2003); and R_c is the corrected thermal radiance using mean values for path radiance, narrow band downward thermal radiation and narrow band transmissivity of air Wukelic et al. (1989). Emissivity values were computed using the NDVI-based algorithm proposed by Jiménez-Muñoz and Sobrino (2003), eliminating the need to use LAI (leaf area index) to estimate emissivity. Corrected thermal radiance (R_c) is derived using an algorithm given by Wukelic et al. (1989) using assumptions reported in Allen et al. (2007). Because the modeling approach evaluates the Ts as a relative ET fraction between the hot/dry and cold/wet boundary values, the consistency of Eq. (5) across space and time is more important than getting the absolute magnitude right.

HESSD
11, 723–756, 2014

Landsat 5 images acquired during the growing season (March to October) were processed to produce Ts maps at a nominal 30 m resolution corresponding to the NDVI resolution although the inherent resolution of the thermal band is 120 m. There were a total of 21 images (10 in 2006; 11 in 2007) available for the 2 yr period over the lysimeter sites. Ts values corresponding to the location of the four lysimeters were extracted. Thus, for each image there were four Ts values from which four ETa estimates were made. This resulted in a total of 84 ETa estimates for the study period (2006–2007).

From the foregoing, four lysimeter ETa measurements (observations) were expected for each image date. However, following the Gowda et al. (2009) study, there were a total of 54 observed lysimeter ETa data points during the same time period (2006–2007); 30 data points in 2006 and 24 in 2007. Out of a total of 54 data points, 28 were from the irrigated fields (NE and SE) while the remaining 26 (NW, SW) were from the dryland lysimeter fields. Thus, only 14 out of 21 images were used for this study due to the unavailability of corresponding observed ETa data. Out of the 14 images used, eight were from 2006 and six from 2007.

2.3 Data analysis

Once the SSEBop computed daily ETa values, according to the simple steps shown in Table 2, the paired lysimeter and modeled ETa data were grouped by treatment (irrigated and dryland) to calculate performance statistics such as mean bias error (MBE), root mean square error (RMSE), and coefficient of determination (R^2). Furthermore, the paired datasets were aggregated by four periods from individual dates (period-1 or "P-1") to "seasonal" aggregation (period-4, "P-4") to indicate the level of aggregation. The "seasonal" aggregation is simply the pooling of the available individual image dates and the corresponding lysimeter data in a given year, but does not constitute an actual integration of daily estimates to seasonal totals.

HESSD
11, 723–756, 2014

2.4 Accuracy assessment

The RMSE provides the overall accuracy of the model that combines the errors from the "bias" (over- or under-estimation) and "precision" (variability or randomness of error). Therefore, error sources were separated into a bias and precision/random component. The precision/random component is quantified and expressed by the mean square variability of the error. Percent contribution of bias vs. precision was evaluated at four aggregation periods namely, period-1 (daily), period-2 (2 day sum), period-3 (3 day sum), and period-4 (sum of all dates in a season). The aggregation was done for each lysimeter and year separately. For example; the NW lysimeter would have aggregation at 1, 2, 3 and seasonal periods for 2006 and 2007. In this case, NW had 14 data points in period-1; but only seven points in period-2, four points in period-3, and two points in period-4 (one each for 2006 and 2007). In total, the aggregation of data generated 54 paired data points in period-1, 26 in period-2, 16 in period-3 and 8 points in period-4.

Like the other periods, the seasonal aggregation was simply the summation of the available daily values for a given lysimeter field, but do not necessarily represent the seasonal total since only a few (6 to 8) data points were available in a given year. Because the objective is to compare modeled vs. observed, we did not use an interpolation technique to estimate the seasonal total.

The mean bias error and random error were investigated separately for irrigated and dryland fields.

$$\mathrm{MBE} = \frac{\sum (M - O)}{N} \tag{6}$$

where MBE is the mean bias error, M is the modeled ET data point, O is the observed lysimeter ET and N is the number of paired data points; $N = 54$, 26, 16 and 8 for period-1, period-2, period-3 and period-4, respectively. The paired data points (N) for

HESSD
11, 723–756, 2014

the irrigated fields were 26 and 24 for the dryland fields.

$$\mathrm{MSE} = \frac{\sum (M - O)^2}{N} \tag{7}$$

where MSE is the mean squared error, RMSE is calculated as the square root of MSE.

Because we know MSE and MBE, the calculation of the square of the random error (MSEe) as the difference between MSE and $(\mathrm{MBE})^2$ can be made by rearranging the following equation:

$$\mathrm{MSE} = \mathrm{MSE}e + (\mathrm{MBE})^2 \tag{8}$$

where, MSEe is the mean square error of the random error term "e", i.e. $(M - O)$ which can be computed alternatively from the error statistics as follows:

$$\mathrm{MSE}e = \frac{\sum (e - \overline{e})^2}{N} \tag{9}$$

$$\overline{e} = \frac{\sum e}{N} = \frac{\sum (M - O)}{N} \tag{10}$$

where $\overline{e}$ is the average of the error term, i.e., $\frac{\sum e}{N}$

MSEe shows the variability of the error itself from the average error. Since the square error terms are additive, the relative contribution of the random error (error variability) and the square of the MBE can be expressed as a percentage of the MSE, which is the total square error between the modeled and observed values.

The accuracy metrics were evaluated for all data points and grouped by irrigation treatment and aggregation periods. Also, when evaluating the entire data points, accuracy metrics were evaluated before and after removing the bias component for the entire dataset and the results are presented in the Tables 3–5.

HESSD
11, 723–756, 2014

3 Results and discussion

The SSEBop approach was evaluated under varying climatic conditions during the spring and summer growing seasons (March to October in 2006 and 2007). Our study site experienced the lowest daily maximum air temperature of 286 K on 4 March 2007 and a high of 312 K on 6 June 2006 with an overall seasonal average of 302 K (Table 1). Similarly, the ETo was lowest on 11 October 2006 with 3.8 mm and highest (7.4 mm) on 7 July 2006 with an overall average of 6.0 mm. The dT was lowest in March and October at about 10 K and peaked in July at about 23 K, with an overall seasonal average of about 19 K. These dT values do not change from year to year for a given day of year.

A step-by-step calculation procedure of the SSEBop approach is presented in Table 2, highlighting the limited data and computational requirements of the method. The illustrative calculation is made for 2007 for one each irrigated (NE) and dryland (NW) lysimeter fields. The 9 columns in Table 2 are required and column 10 shows the observed lysimeter data. The steps are simple and straightforward to follow. The cold boundary condition (Tc) was obtained by multiplying the daily maximum air temperature by 0.983. This correction is necessary and was determined by comparing Ts of the "cold" pixels (those with NDVI > 0.8) with that of the maximum air temperature in the corresponding pixels. These values tend to be steady throughout the growing season but need to be evaluated and established for the sensor or Ts estimation method used (MODIS vs. Landsat and different assumptions for emissivity can produce different Ts within a sensor). The correction coefficient enables the conversion of the daily maximum air temperature into a cold boundary condition, eliminating the requirement to select cold pixels from the image, which are sometimes difficult to find. Furthermore, the use of air temperature expands the geographical applicability of the approach since the calculation procedure is not restricted to the hydro-climatic region of the reference cold/hot pixels. In this case, every pixel has its own hot/cold reference points. The hot boundary condition is obtained by adding the dT as is shown in column 5 (Table 2).

HESSD
11, 723–756, 2014

Because of the close proximity of the four lysimeters, the cold and hot boundary conditions were identical for all fields, so the only difference is the Ts for each field. As expected, the irrigated lysimeter field (NE) experienced cooler Ts on most days compared to the dryland lysimeter field (NW). For example, during the peak growing season (26 July 2007), the irrigated NE field was 302 K while the dryland NW field was 308 K. On two dates where the NW field was cooler than the NE field, the difference in temperature was less than or equal to 2 K, which is close to the required accuracy level of Ts and/or modeled ET estimates in similar surface energy balance applications (Su, 2002).

The relationships between Ts and the boundary conditions and the resulting ETa are shown in Figs. 2 and 3 for the irrigated and dryland lysimeter fields, respectively. The top portions of these charts show that the observed Ts lies between the Th and Tc boundary conditions. The bottom portions of the charts show the corresponding modeled ETa and observed estimates. During the early part of the season (March–June), the Ts was found close to the hot boundary line, which resulted in a lower ETa. During the peak season (July and August), the Ts was found close to the cold boundary condition, resulting in an ET fraction close to 1.0, and thus resulting in higher ETa (driven by the higher ETo).

During the early parts of the growing season, Ts values were plotted beyond the hot boundary line, resulting in a negative ET fraction. For example, in March and April 2006, i.e., Ts was warmer than Th. Although it is possible that the hot boundary condition can be cooler than Ts in some desert landscapes when compared to agricultural reference conditions due to high albedo, in this approach, each pixel has its own reference boundary conditions and we do not anticipate the Ts to be warmer than the Th. Thus, it is possible that either the Tc was too low or the dT estimate was too small or both. Since this situation occurred in the early season where ET is small, the overall contribution to seasonal estimates is minimal. The method is also a simplified method that does not take into account ground heat flux and sensible heat partitioning; thus, making it subject for such potential errors in some instances. More evaluation is warranted to

HESSD
11, 723–756, 2014

verify if similar early-season problems occur in other parts of the CONUS and around the world. Despite such limitations, the method captures the major seasonal variations in ET both in trend and magnitude. For example, on 23 July 2006, the Ts indicated a sudden increase in magnitude on both the irrigated (NE) and dryland (NW) lysimeter fields, and that effect appears to be correctly calculated with a lower modeled ETa as evidenced by the observed ETa patterns (Figs. 2 and 3).

Time series of both modeled and observed ETa, grouped by water management practice and year are shown in Fig. 4 for all 54 data points. The modeled ETa corresponded well with the trend and magnitudes of the observed ETa with no apparent differences in performance between irrigated and dryland lysimeter fields or between years. However, the model results show a general under-estimation by the SSEBop model (Table 3). This under-estimation bias is calculated to be $-0.43\,\mathrm{mm\,d^{-1}}$ or 11 % of the daily mean value when all data points are considered (Table 3). The under-estimation bias was $-0.34\,\mathrm{mm\,d^{-1}}$ (8 %) for irrigated and $-0.52\,\mathrm{mm\,d^{-1}}$ (14 %) for dryland fields; however, the RMSE was 32 %, 28 %, and 25 % of the mean daily values for the dryland, combined, and irrigated fields, respectively.

The separation of the error into bias and random components provides further useful information. Note that the square of bias errors and the error variance (random) add up to the mean square error (MSE) according to Eq. (6). Using MSE as the overall total error, irrigated fields show relatively lower bias errors ($\mathrm{MBE}^2 = 0.12$) and higher random errors (MSEe) of 1.11, which are 9 % and 91 % of the MSE (1.22). On the other hand, dryland fields show a relatively higher bias (MBE^2: 0.27, 20 %) and comparable random error as the irrigated fields (1.10, 80 %) with an overall comparable MSE (1.37). Similarly, when irrigated and dryland fields were combined, the contribution of the bias error was 14 % while the random error was 86 % of the total error. Thus, at the daily scale analysis, the random error contribution was much higher than the bias error contribution (to the total error), which can be expressed by the RMSE as 1.14 mm or 28 % of the mean daily value.

HESSD
11, 723–756, 2014

Because of the relatively higher RMSE (28 %) at the daily time scale, we aggregated the paired data points at 2-day, 3 day and seasonal periods and calculated the different error components. Table 4 shows error statistics (period-1 to 4) with the original data while Table 5 shows the same error statistics after a bias correction (12 % increase) was applied to the modeled ETa. The bias correction was defined as the ratio of mean observed ETa (4.07 mm) to mean modeled ETa (3.64 mm) using all 54 data points.

The mean ETa values (both modeled and observed) increased as we aggregated the data points over time as expected from 4.1/3.6 to 27.4/24.6 mm for the observed/modeled ETa (Table 4). On the other hand, the mean bias percentage (MBE %) remained about the same at 11 % while the RMSE decreased from 28 to 12 %. When we differentiate the contributions of the two error components, the mean bias error square (MBE^2) increased from 14 % at period-1 to 80 % at the seasonal scale while the random (MSE*e* %) decreased from 86 to 20 % for the same time periods. The temporal evolution of bias and random error contributions is shown in Fig. 5, illustrating the impact of temporal aggregation on modeling/data errors.

The scatterplot of the four aggregation periods is shown in Fig. 6a–d. The scatterplots show a strong linear association between modeled and observed ETa with R^2 ranging from 0.87 to 0.97 at different aggregation periods. The reason for the differences in R^2 between the aggregation periods is difficult to explain due to differences in the number of data points, ranging from 8 to 54. Also, due to the clumping of data points close to period-average values, period-3, Fig. 6c, produced a high R^2 (0.97). Therefore, it is more meaningful to evaluate the MBE and RMSE than R^2 under such circumstances. However, the strong linear relationship between the model and observed data at all aggregation levels indicates that the SSEBop's approach in the calculation of the ET fraction (ET_f) using a linear assumption between hot and cold boundary conditions is valid. The difference in magnitude between the irrigated and dryland fields becomes clearer as the aggregation periods increase. As expected, on average, the irrigated fields show higher ET values than the dryland fields (Table 3 and Fig. 6).

HESSD
11, 723–756, 2014

Two important conclusions can be made from the aggregation analyses (Table 4 and Fig. 6): (1) RMSE error that may appear discouraging at the daily time scale (28 %) becomes more acceptable as we aggregate the data to a seasonal ET estimate (RMSE = 12 %) The reason for the improvement of RMSE with aggregation is because the high random components of the error at daily scale tend to cancel each other as we pool more data points together; and (2) although the bias error appeared to be small at the daily time scale, dominated by the random error, the bias remains persistent and directional, becoming a dominant error source as we aggregate the data at seasonal time scales. Thus, it is important to identify the sources of bias and remove or reduce the bias especially when the model is used in water balance calculations. The importance of the bias correction is less critical if the model is used to detect relative changes for applications such as drought monitoring.

The bias factor was determined to be 1.12, i.e., the observed ETa was about 12 % higher than the modeled ETa. The source of this bias could be related to the combination of the magnitude of ETo used and the inherent SSEBop setup such as the dT magnitude or the use of a constant air temperature correction factor. Further research is required to conclusively identify the source of the bias. However, it was encouraging to see that a simple bias correction can be applied to improve the results.

As shown in Table 5, applying the bias correction would remove the bias error contribution with little change to the random error component. The RMSE improved slightly for the first three aggregation periods but showed a substantial reduction at seasonal scale from 12 to 6 %. The removal of the bias error is important since we avoid directional under- or over-estimation, both of which affect critical water resources decisions such as water allocation and curtailment. Obviously, for the same RMSE, a model with no bias is superior to a model with a bias since the random errors that dominate the RMSE will tend to compensate over time or space, thus conserving volumetric estimates.

Overall, this study demonstrates that modeled ET using the SSEBop approach produced a comparable, if not improved, result in comparison to the manual hot and cold

HESSD
11, 723–756, 2014

pixel approach of SSEB that Gowda et al. (2009) reported with the same lysimetric data. While they reported an RMSE of 1.2 mm with a gross over-estimation on dryland fields, this study finds an RMSE 1.14 mm (28 %) and a slightly higher under-estimation bias (−0.52 mm) with dryland fields compared to the −0.34 mm bias with irrigated fields. Overall, the SSEBop shows a comparable performance between irrigated and dryland fields with a seasonal RMSE at 12 % (biased) and 6 % (unbiased). Furthermore, Senay et al. (2013) applied the SSEBop using MODIS data streams and evaluated it using 45 flux tower eddy covariance monthly datasets distributed across the CONUS; the analysis produced comparable relationships with a nationwide R^2 of 0.64 but with a much higher R^2 value (> 0.8) at selected flux-tower stations. Velpuri et al. (2013) also validated the MODIS-based SSEBop for the CONUS using multi-year point and gridded eddy covariance flux tower and water-balance-based approaches and concluded that it has the potential to be used for hydrologic and drought monitoring applications.

Performance results from this study strengthen the useful application of the SSEBop approach for quick and robust estimation of ET using satellite-based Ts regardless of the type of thermal sensor. This method can easily be applied to the recently launched LDCM (Landsat Data Continuity Mission) satellite data with its improved TIRS bands. The overall RMSE accuracy of the model (6 to 25 %) falls within the reported error ranges as summarized by Allen et al. (2011b) and Gowda et al. (2008) for remote-sensing-based surface energy balance models (5 to 30 %). SSEBop can be applied with a high degree of consistency for users who have limited experience in surface energy balance modeling but understand the fundamentals of ET and image processing.

4 Conclusions

The main objective of this study was to evaluate the performance of the operational simplified surface energy balance (SSEBop) model using lysimetric data that were used in the evaluation of an earlier version of the model, which entailed a manual hot and cold pixel selection approach. The SSEBop approach is arguably one of the most

HESSD
11, 723–756, 2014

simplified of all surface energy balance modeling techniques that can be used for both local and regional ET mapping. The SSEBop approach requires only satellite-based land surface temperature (Ts) along with a point or gridded reference ET (ETo) and air temperature (Ta) datasets. Users can quickly estimate actual ET using pre-defined hot and cold differential temperatures (dT) as soon as Ts, Ta and ETo are available. The method does not require setting up hot and cold reference pixels, thus making the method scalable from local to regional extents, i.e., each pixel has its own hot and cold boundary conditions, whose dT is pre-defined.

This study demonstrated that SSEBop produced comparable results to that of the SSEB method in terms of RMSE, but with an improved bias error. The gross over-estimation that was observed with the SSEB on dryland fields was not reproduced under SSEBop. Generally, the performance between irrigated and dryland fields was comparable with an overall under-estimation bias of around 11 %.

Temporal analysis of the errors showed that the RMSE decreased from a high of 28 % at the daily time scale to 12 % at a seasonal time scale, highlighting the importance of time scale in evaluating accuracy levels of ET models. Because large-scale irrigation water management is concerned with seasonal water use estimations, such relatively low seasonal RMSE should build confidence in the use of remote-sensing-based ET. With further removal of the bias, the seasonal RMSE percentage decreased to 6 %.

The two error components moved in opposite directions as the aggregation period increased. For example, the contribution of the random error (MSEe) to the total error decreased (86 to 20 %) while that of the bias error (MBE^2) increased (11 to 80 %). Although the ratio of bias error to mean observed value remained at about 11 % throughout the aggregation period, its proportional contribution to the total error sources increased with the period of aggregation. In short, while estimating a given day's ET had a high uncertainty error (around 28 % of the mean value), a seasonal ETa estimate was made with a less than 10 % error.

HESSD
11, 723–756, 2014

This study highlights the fact the SSEBop can be effective and produce reliable ET estimates at the scale of the available remotely sensed thermal data. However, it is important to understand the relationships between the two error components and their impacts on the overall accuracy and usefulness of the model for the intended purpose.

Considering the simplicity of the modeling concept and operational implementation, the SSEBop is a promising approach for users who are interested in estimating ET operational applications using remotely sensed data but do not want to solve the full energy balance equation.

Acknowledgement. Note: the use of trade, firm, or corporation names in this article is for the information and convenience of the reader. Such use does not constitute an official endorsement or approval by the United States Geological Survey or the United States Department of Agriculture or the Agricultural Research Service of any product or service to the exclusion of others that may be suitable.

References

Allen, R. G.: REF-ET: Reference Evapotranspiration Calculation Software for FAO and ASCE Standardized Equations (Version 3.1.), University of Idaho, Boise, Idaho, 2011.

Allen, R. G., Pereira, L. S., Raes, D., and Smith, M.: Crop evapotranspiration: guidelines for computing crop water requirements, in: Irrigation and Drainage Paper 56, FAO, Rome, Italy, 1998.

Allen, R. G., Tasumi, M., and Trezza, R.: Satellite-based energy balance for mapping evapotranspiration with internalized calibration (METRIC) – model, J. Irrig. Drain. E.-ASCE, 133, 380–394, 2007.

Allen, R. G., Pereira, L. S., Howell, T. A., and Jensen, M. E.: Evapotranspiration information reporting: I. Factors governing measurement accuracy, Agr. Water Manage., 98, 899–920, doi:10.1016/j.agwat.2010.12.015, 2011.

Anderson, M. C., Norman, J. M., Diak, G. R., Kustas, W. P., and Mecikalski, J. R.: A two-source time-integrated model for estimating surface fluxes using thermal infrared remote sensing, Remote Sens. Environ., 60, 195–216, 1997.

HESSD

11, 723–756, 2014

ASCE: The ASCE Standardized Reference Evapotranspiration Equation, Task Committee on Standardization of Calculation of Reference ET, Environment and Water Resources Institute 200, Reston, Virginia, 2005.

Bastiaanssen, W. G. M., Menenti, M., Feddes, R. A., and Holtslag, A. A. M.: The surface energy balance algorithm for land (SEBAL): Part 1 formulation, J. Hydrol., 212–213, 198–213, 1998.

Chavez, J. L., Gowda, P. H., Howell, T. A., and Copeland, K. S.: Radiometric surface temperature calibration effects on satellite based evapotranspiration estimation, Int. J. Remote Sens., 30, 2337–2354, 2009.

Gowda, P. H., Chavez, J. L., Colaizzi, P. D., Evett, S. R., Howell, T. A., and Tolk, J. A.: ET mapping for agricultural water management: present status and challenges, Irrigation Sci., 26, 223–237, 2008.

Gowda, P. H., Senay, G. B., Colaizzi, P. D., and Howell, T. A.: Lysimeter validation of the Simplified Surface Energy Balance (SSEB) approach for estimating actual ET, T. ASABE, 25, 665–669, 2009.

Gowda, P. H., Ennis, J. R., Howell, T. A., Marek, T. H., Porter, D. P., and Dusek, D. A.: Bushland Reference ET Calculator, USDA-ARS Conservation and Production Research Laboratory, Bushland, Texas, 2011.

Howell, T. A., Schneider, A. D., Marek, T. H., and Steiner, J. L.: Calibration and scale performance of Bushland weighing lysimeters, T. ASAE, 38, 1019–1024, 1995.

Kalma, J. D., McVicar, T. R., and McCabe, M. F.: Estimating land surface evaporation: a review of methods using remotely sensed surface temperature data, Surv. Geophys. 29, 421–469, 2008.

Kanamitsu, M.: Description of the NMC global data assimilation and forecast system, Weather Forecast., 92, 847–854, 1989.

Kustas, W. P. and Norman, J. M.: A two-source energy balance approach using directional radiometric temperature observations for sparse canopy covered surfaces, Agron. J., 92, 847–854, 2000.

Moran, M. S., Rahman, A. F., Washburne, J. C., Goodrich, D. C., Weltz, M. A., and Kustas, W. P.: Combining the Penman–Monteith equation with measurements of surface temperature and reflectance to estimate evaporation rates of semiarid grassland, Agr. Forest Meteorol., 80, 87–109, 1996.

Mu, Q., Zhao, M., and Running, S. W.: Improvements to a MODIS global terrestrial evapotranspiration algorithm., Remote Sens. Environ., 115, 1781–1800, 2011.

HESSD
11, 723–756, 2014

Oberg, J. W. and Melesse, A. M.: Evapotranspiration dynamics at an ecohydrological restoration site: an energy balance and remote sensing approach, J. Am. Water Resour. As., 42, 565–582, doi:10.1111/j.1752-1688.2006.tb04476.x, 2006.
Porter, D. O., Gowda, P. H., Marek, T. H., Howell, T. A., Irmak, S., and Moorhead, J.: Sensitivity of grass and alfalfa reference evapotranspiration to sensor accuracy, Appl. Eng. Agric., 28, 543–549, 2012.
Roerink, G. J., Su, Z., and Menenti, M.: A simple remote sensing algorithm to estimate the surface energy balance., Phys. Chem. Earth, 25, 147–157, 2000.
Senay, G. B., Budde, M., Verdin, J. P., and Melesse, A. M.: A coupled remote sensing and simplified surface energy balance approach to estimate actual evapotranspiration from irrigated fields, Sensors, 7, 979–1000, 2007.
Senay, G. B., Leake, S., Nagler, P. L., Artan, G. A., Dickinson, J., Cordova, J. T., and Glenn, E. P.: Estimating basin scale evapotranspiration (ET) by water balance and remote sensing methods, Hydrol. Process., 25, 4037–4049, doi:10.1002/hyp.8379, 2011.
Senay, G. B., Bohms, S., Singh, R. K., Gowda, P. H., Velpuri, N. M., Alemu, H., and Verdin, J. P.: Operational evapotranspiration mapping using remote sensing and weather datasets: a new parameterization for the SSEB approach, J. Am. Water Resour. As., 49, 577–591, doi:10.1111/jawr.12057, 2013.
Sobrino, J. A., Jiménez-Muñoz, J. C., and Paolini, L.: Land surface temperature retrieval from LANDSAT TM 5, Remote Sens. Environ., 90, 434–440, 2004.
Su, Z.: The Surface Energy Balance System (SEBS) for estimation of turbulent heat fluxes, Hydrol. Earth Syst. Sci., 6, 85–100, doi:10.5194/hess-6-85-2002, 2002.
Thenkabail, P. S.: Biophysical and yield information for precision farming from near-real time and historical Landsat TM images, Int. J. Remote Sens., 24, 2879–2904, 2003.
Thornton, P. E., Thornton, M. M., Mayer, B. W., Wilhelmi, N., Wei, Y., and Cook, R. B.: Daymet: daily surface weather on a 1 km grid for North America, 1980–2008, Oak Ridge National Laboratory, Oak Ridge, Tennessee, 2012.
Tucker, C. J.: Red and photographic infrared linear combinations for monitoring vegetation, Remote Sens. Environ., 8, 127–150, 1979.
Velpuri, N. M., Senay, G. B., Singh, R. K., Bohms, S., and Verdin, J. P.: A comprehensive evaluation of two MODIS evapotranspiration products over the conterminous United States: Using point and gridded FLUXNET and water balance ET, Remote Sens. Environ., 139, 35–49, doi:10.1016/j.rse.2013.07.013, 2013.

HESSD
11, 723–756, 2014

Wan, Z. and Li, Z.: A physics-based algorithm for retrieving land-surface emissivity and temperature from EOS/MODIS data, IEEE T. Geosci. Remote, 35, 980–996, 1997.
Wukelic, G. E., Gibbons, D. E., Martucci, L. M., and Foote, H. P.: Radiometric calibration of Landsat thematic mapper thermal band, Remote Sens. Environ., 28, 339–347, 1989.
Xie, P. and Arkin, P. A.: A 17-year monthly analysis based on gauge observations, satellite estimates, and numerical model outputs, B. Am. Meteorol. Soc., 78, 2539–2558, 1997.

HESSD
11, 723–756, 2014

Table 1. Summary of reference ET (ETo), maximum air temperature (Ta_max) and dT datasets during the 21 Landsat image dates at the Bushland weather station. DOY is the julian date for the day of year.

Date	DOY	Ta_max (K)	ETo (mm)	dT (K)
18 Apr 2006	108	297	6.03	17.59
20 May 2006	140	309	6.16	21.19
5 Jun 2006	156	312	6.80	22.58
21 Jun 2006	172	309	4.86	23.33
7 Jul 2006	188	303	7.36	23.46
23 Jul 2006	204	307	6.94	22.69
8 Aug 2006	220	306	6.31	21.48
24 Aug 2006	236	306	6.12	19.34
25 Sep 2006	268	297	4.81	13.26
11 Oct 2006	284	295	3.85	10.25
4 Mar 2007	63	286	4.29	9.72
7 May 2007	127	293	6.57	19.65
23 May 2007	143	301	6.51	21.19
8 Jun 2007	159	296	7.32	22.58
24 Jun 2007	175	304	6.80	23.33
10 Jul 2007	191	307	6.89	23.46
26 Jul 2007	207	305	6.77	22.69
11 Aug 2007	223	308	6.61	21.48
27 Aug 2007	239	305	6.14	19.34
12 Sep 2007	255	300	4.83	16.41
28 Sep 2007	271	302	4.76	13.26
Average	–	302	6.03	19.44

HESSD
11, 723–756, 2014

Table 2. SSEBop calculation procedures using irrigated (NE) and dryland (NW) fields for 2007 as an example.

Plot	Date	1 Ta	2 *c*	3 Tc 1 × 2	4 dT	5 Th 3 + 4	6 Ts	7 ET_f (5–6)/4	8 ETo	9 ETa_m 7 × 8 × 1.25	10 ETa_o
NE	4 Mar	286	0.983	281	10	291	296	0.00	4.3	0.0	0.4
	23 May	301	0.983	296	21	317	310	0.33	6.5	2.7	4.1
	8 Jun	296	0.983	291	23	314	313	0.04	7.3	0.4	1.1
	10 Jul	307	0.983	302	23	325	308	0.74	6.9	6.4	7.3
	26 Jul	305	0.983	300	23	323	302	0.91	6.8	7.7	6.7
	11 Aug	308	0.983	303	21	324	303	1.00	6.6	8.2	7.4
NW	4 Mar	286	0.983	281	10	291	294	0.00	4.3	0.0	0.3
	23 May	301	0.983	296	21	317	313	0.19	6.5	1.5	0.1
	8 Jun	296	0.983	291	23	314	312	0.09	7.3	0.8	1.2
	10 Jul	307	0.983	302	23	325	315	0.43	6.8	3.7	5.4
	26 Jul	305	0.983	300	23	323	308	0.65	6.9	5.6	5.9
	11 Aug	308	0.983	303	21	324	305	0.90	6.6	7.4	7.6

Note: Column 9 is a product of columns 7 and 8 and the "alfalfa" correction factor 1.25. For clarity several columns have been rounded to whole numbers. ETa_m is modeled and ETa_o is observed.

HESSD
11, 723–756, 2014

Table 3. Accuracy assessment and error statistics by irrigation type.

	Irrigated (n = 28)	Dryland (n = 26)	Combined (n = 54)
ETa_m/ETa_o	4.1/4.4	3.2/3.7	3.6/4.1
MBE (%)	−0.34(8)	−0.52(14)	−0.43(11)
RMSE (%)	1.11(25)	1.17(32)	1.14(28)
R^2	0.89	0.86	0.87
MSE	1.22	1.37	1.29
MBE^2 (%)	0.12(9)	0.27(20)	0.18(14)
MSEe (%)	1.11(91)	1.10(80)	1.10(86)

Note: ETa_m/ET_o are modeled and observed ETa. Numbers in bracket are errors expressed in percent of the observed ETa. MBE and RMSE are in mm; MSE, MBE^2 and MSEe are variances in units of mm^2. "n" is the number of paired data points.

HESSD
11, 723–756, 2014

Table 4. Accuracy assessment and error statistics by four aggregation periods. P-1, P-2, P-3, and P-4 correspond to 1, 2, 3 day and "seasonal" periods.

	P-1 (n = 54)	P-2 (n = 26)	P-3 (n = 16)	P-4 (n = 8)
ETa_m/ETa_o	3.6/4.1	7.3/8.2	11.1/12.7	24.6/27.4
MBE (%)	−0.43(11)	−0.92(11)	−1.63(13)	−2.88(11)
RMSE (%)	1.14(28)	1.98(24)	2.04(16)	3.23(12)
R^2	0.87	0.88	0.97	0.90
MSE	1.29	3.94	4.14	10.46
MBE^2 (%)	0.18(14)	0.84(21)	2.66(64)	8.31(80)
MSEe (%)	1.10(86)	3.10(79)	1.48(36)	2.14(20)

Note: ETa_m/ET_o are modeled and observed ETa. Numbers in bracket are errors expressed in percent of the observed ETa. MBE and RMSE are in mm; MSE, MBE^2 and MSEe are variances in units of mm^2. "n" is the number of paired data points.

HESSD
11, 723–756, 2014

Table 5. Bias corrected Accuracy Assessment and Error statistics by four aggregation periods (1, 2, 3 day and "seasonal") after removing bias using a factor of 1.2.

	P-1 (n = 54)	P-2 (n = 26)	P-3 (n = 16)	P-4 (n = 8)
ETa_m/ETa_o	4.1/4.1	8.2/8.2	12.4/12.7	27.5/27.4
MBE (%)	0.00(0)	0.00(0)	−0.30(2)	0.10(0)
RMSE (%)	1.13(28)	1.91(23)	1.63(13)	1.71(6)
R^2	0.87	0.88	0.97	0.90
MSE	1.28	3.64	2.67	2.93
MBE^2 (%)	0.00(0)	0.00(0)	0.09(3)	0.00(0)
MSEe (%)	1.28(100)	3.64(100)	2.58(97)	2.93(100)

Note: ETa_m/ET_o are modeled and observed ETa. Numbers in bracket are errors expressed in percent of the observed ETa. MBE and RMSE are in mm; MSE, MBE^2 and MSEe are variances in units of mm^2. "n" is the number of paired data points.

HESSD
11, 723–756, 2014

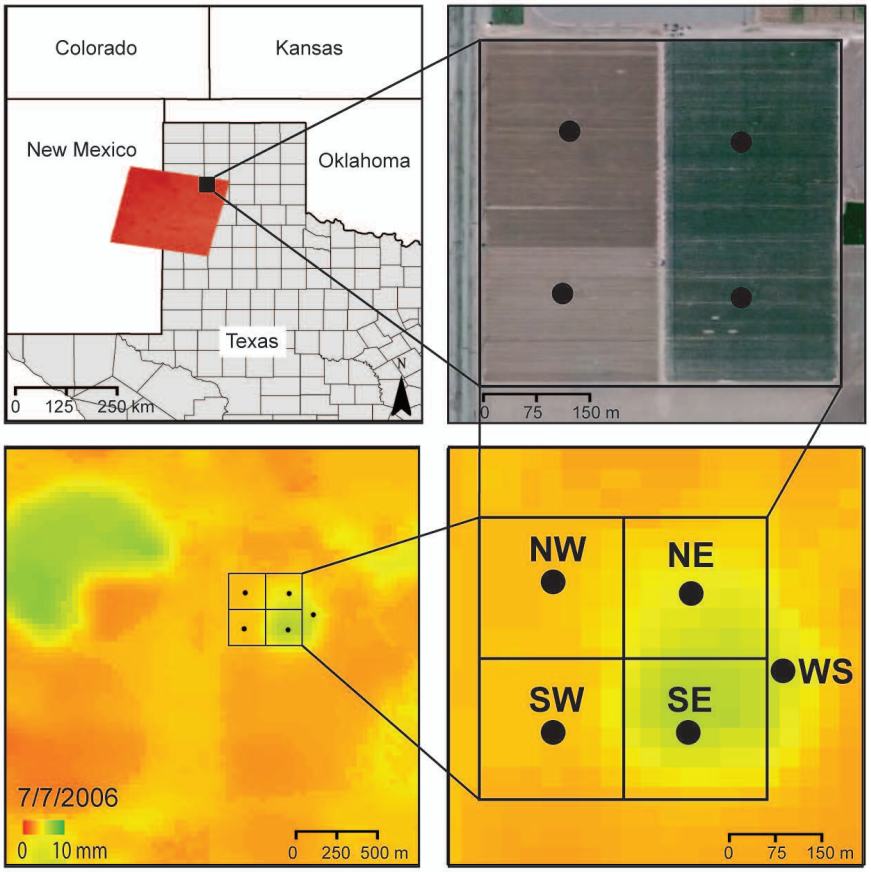

Fig. 1. Study site. Color map shows SSEBop modeled ETa distribution for 7 July 2006. Lysimeter fields are designated as NW, NE, SE and SW. NE and SE are Irrigated and NW and SW are dyrland. WS shows the location of the Bushland weather station. The dark dots approximate the location of actual lysimeter or weather station.

HESSD
11, 723–756, 2014

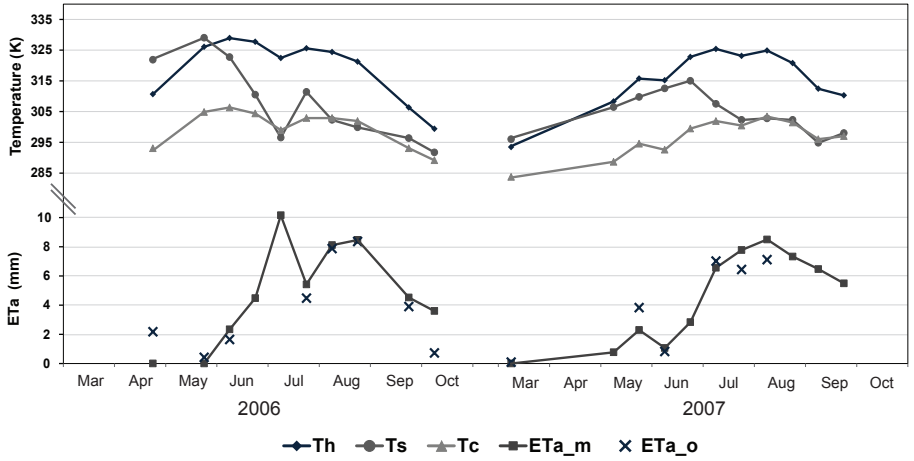

Fig. 2. Temporal evolution of hot (Th) and cold (Tc) boundary conditions along with observed land surface temperatures (Ts). Also shown are modeled (ETa_m) and observed (ETa_o) ETa for the irrigated (NE) lysimeter site.

HESSD
11, 723–756, 2014

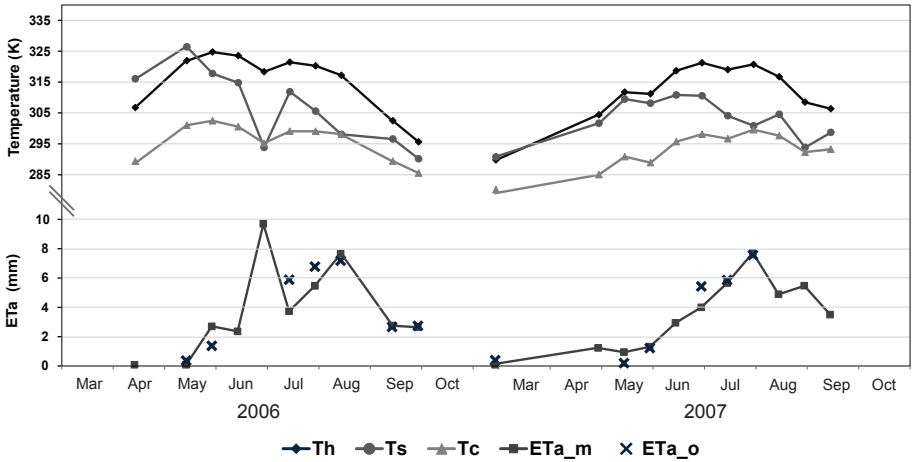

Fig. 3. Temporal evolution of hot (Th) and cold (Tc) boundary conditions along with observed land surface temperatures (Ts). Also shown are modeled (ETa_m) and observed (ETa_o) ETa for the dryland (NW) lysimeter site.

HESSD
11, 723–756, 2014

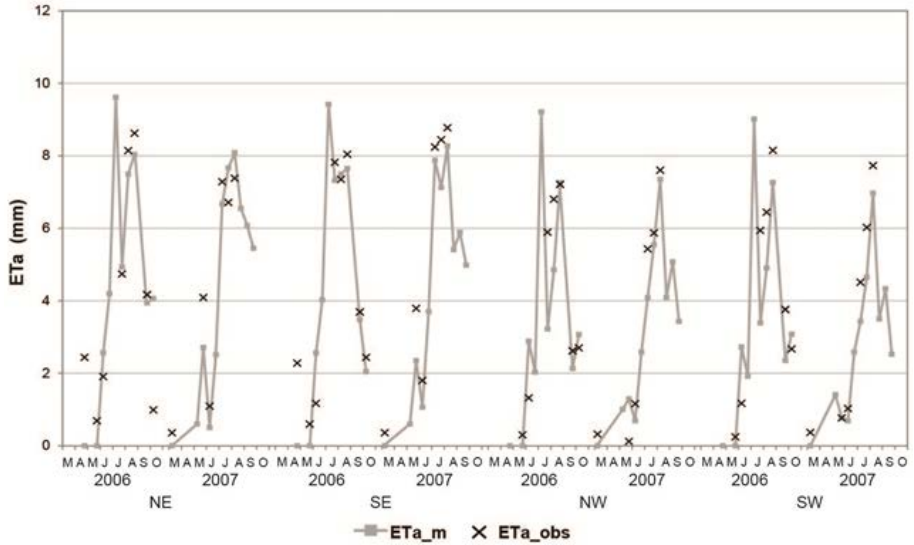

Fig. 4. Observed (ETa_o) and modeled (ETa_m) ETa for all four Lysimeter fields, grouped by field and year.

HESSD
11, 723–756, 2014

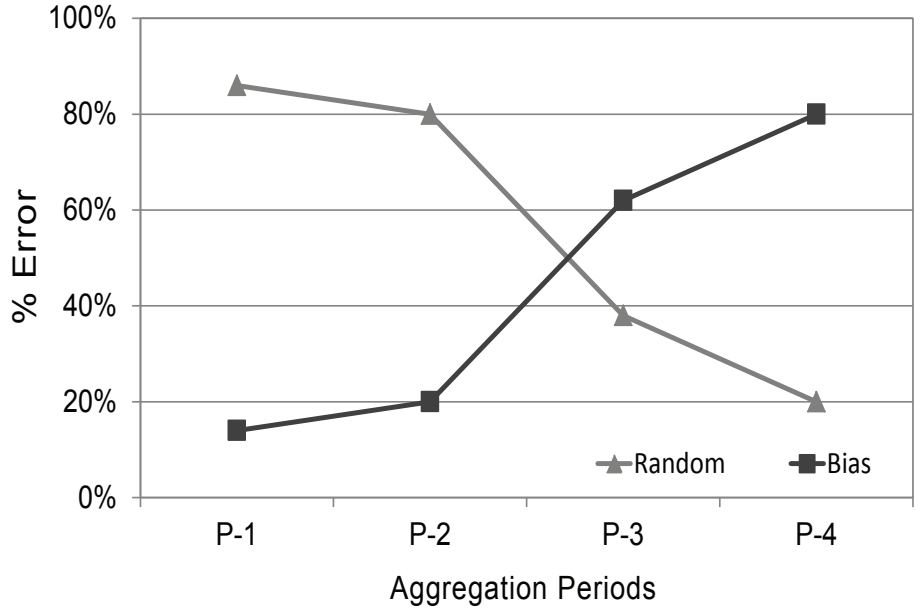

Fig. 5. The temporal relationships between bias and random error components as a result of varying temporal aggregation scales. P-1: no aggregation (daily); P-2: two-day aggregation; P-3: three-day aggregation; P-4: "seasonal" aggregation. Percent error shows component contribution from the total mean square error.

HESSD
11, 723–756, 2014

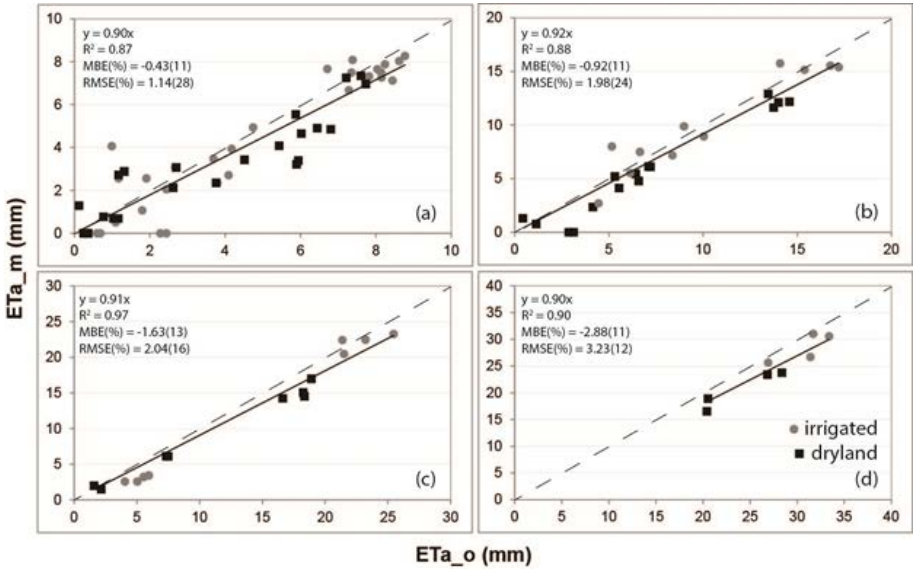

Fig. 6. Scatterplot between modeled (ETa_m) and observed (ETa_o) ETa at four aggregation periods: **(a)** individual point (non-aggregation) with $n = 54$; **(b)** and **(c)** P-2 and P-3 with 2 and 3 aggregation dates ($n = 25$ and $n = 16$); **(d)** P-4 (seasonal) aggregation with $n = 8$. MBE (bias) and RMSE error and their percentages from their respective means are shown in brackets. Because the intercept was very small (0.001, "a"), we forced the best-fit line through the origin.

HESSD
11, 723–756, 2014